Investigation of the Supersonic Flow Field around a delta wing using Particle-Image-Velocimetry

N. Lang

Aerodynamisches Institut, RWTH—Aachen, Wüllnerstr. zw. 5 u. 7, D-52062 Aachen, Germany
Tel.: ++49+241/805426, Fax: ++49+241/8888257, E-Mail: neven@aia.rwth-aachen.de

ABSTRACT

Hypersonic flight vehicles as e.g. space transportation systems are designed as delta wings. The ELAC configuration was designed as such a transport system for future orbital missions. Its first stage is a lifting-body system, which carries a second orbital stage up to an altitude of ~30 km at $Ma_\infty = 7$. At positive angles of attack flow separates near to these leading edges and generates vortices at the leeward side of the wing. The flow at the leeward side of the wing in supersonic flow is subject of this investigation. First a combination of oil-flow pattern and Vapour-Screen is applied to obtain quantitative results about the flow field. Oil flow pattern show a "fingerprint" of the flow near to the body surface. Its structure indicates separation lines and the areas of reattachment of the flow. In addition to this the Vapour-Screen method shows vortices in the flow field. Combining both methods qualitative results are obtained as shown in figure 1a. The upper part of figure 1a describes a front view of the Vapour-Screen. The dark area indicates the primary vortex, which is caused by flow separation near to the leading edge. A top view on the wing is shown in the lower part of Figure 1a. Flow separation near the leading edge and reattachment of the flow at the left hand side can clearly be seen. Understanding of the flow phenomena allows an appropriate design of quantitative measurement techniques as for example Particle-Image-Velocimetry. This technique is being used to gain also quantitative information about the velocity distribution in the flow field. Light-sheets are adjusted in main flow direction. A combination of the results from a set of measurements in parallel and perpendicular planes leads to a dataset containing all velocity components in the three-dimensional flow field. The spatial development of leading edge vortices can be therefore described. Figure 1b shows the *x*-component of vorticity, which was computed out of the measured velocities. Four planes in downstream direction depict the vorticity distribution perpendicular to the free stream direction. The applied experimental techniques are also used for validation of results from numerical simulation.

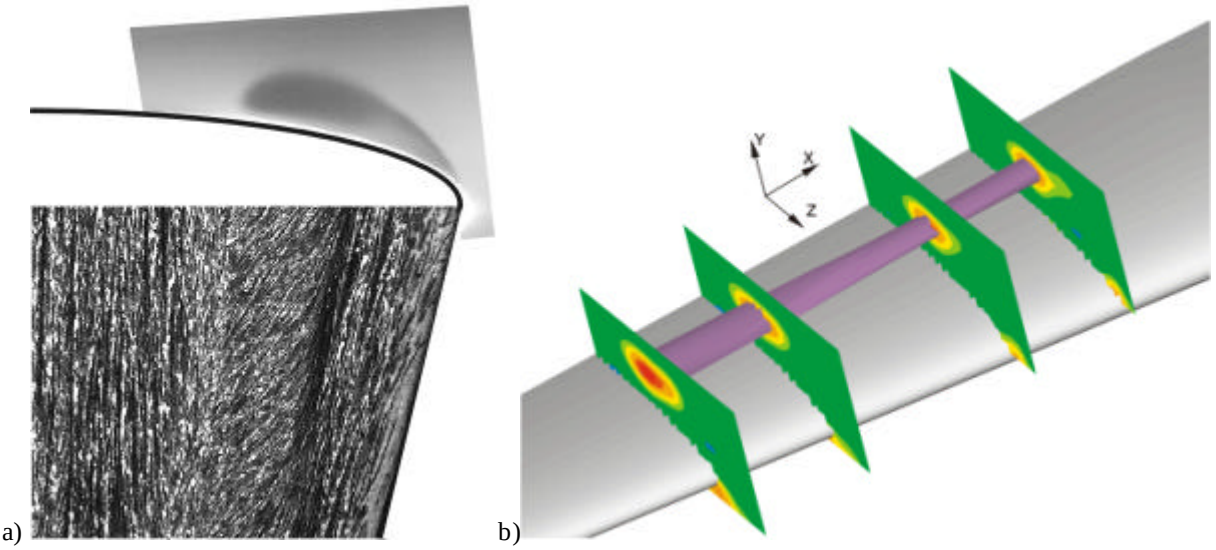

Figure 1: a) Oil flow pattern (upper part) and Vapour-Screen (lower part) at the leeward side of the delta wing configuration ELAC at $Ma_\infty = 2$, $\alpha = 10°$ at x/l = 30% ($Re_\infty = 8.9 \cdot 10^6$). b) Vorticity distribution over the leeside of the delta wing configuration ELAC in four planes perpendicular to the free stream direction and extracted isosurface of constant vorticity. Vorticity was computed out of PIV-measurements at Ma = 2 and $\alpha = 10°$ ($Re_\infty = 3.7 \cdot 10^6$).

1. INTRODUCTION

Present space transportation systems can be divided in three objectives: Development of new techniques, military applications and commercial applications. The number of commercial missions will increase tremendously in next future. For example from 1996 to 1997 the number of commercial missions increased by a factor of 3. From 1998 to 2004 approximately 1200 communication satellites will be put into operation. The development of the presently used transportation systems was initiated by several governments for military aims. Therefore costs and financial efficiency were of less importance.

Plans for future space transportation systems will therefore follow new concepts. Improvements will be achieved in cost reduction, safety during mission, operational flexibility, reuse and reduction of pollution. The two-stage-to-orbit vehicles (TSTO) are estimated to have a high potential concerning these demands. They consist of two vehicles. The first stage is designed as a hypersonic lifting body configuration, which starts horizontally and carries the second orbital stage up to an altitude of ~30 km. Then the second stage is separated and flies into the orbit to drop the payload. Such a TSTO-system was developed in the Collaborative Research Center "Fundamentals of Design of Aerospace Planes" of the German research association DFG. The first stage ELAC is a delta shaped wing with rounded leading edges, see Figure 2.

Figure 2: Two-stage-to-orbit vehicle with the first stage ELAC and the second orbital stage EOS. ELAC is designed as a hypersonic flight vehicle, which takes off horizontally and flies up to an altitude of ~30 km, where it comes up to Ma = 7.

Delta shaped wings are used for supersonic flight to reduce the effects of compressibility. At positive angles of attack flow separates at the sharp leading edges and rolls up into vortex sheets over the leeside of the wing. This strong interaction causes additional lift, the so-called vortex-lift, and an increased manoeuvrability. The structure of the leeside flow has been characterized for delta wings with sharp leading edges. Dependent on the angles of attack normal to the leading edges α_N and the Mach number Ma_N Miller and Wood (1984) defined different classes for delta wings with sharp leading edges.

The ELAC configuration was designed with rounded leading edges to reduce heat flux in the hypersonic flight regime. Therefore the classification of Miller and Wood (1984) must be checked concerning its applicability, because the nose radius has a large effect on flow separation.

Due to this the present study deals with the investigation of the leeside flow field of the first stage ELAC. Wind tunnel tests were carried out in supersonic flow, because the delta wing passes through all speed regimes from incompressible flow, transonic flow, supersonic flow up to hypersonic flow during mission. First the flow field is visualized for a qualitative investigation. The results are used to design a proper set-up for quantitative measurements. All used techniques are non-intrusive to avoid any disturbances of the flow.

Flow visualization is performed by the use of Vapour-Screen and oil flow pattern. The oil flow pattern shows the areas of flow separation and reattachment. Between the lines of separation and reattachment the direction of the flow near to the body surface is indicated. This "fingerprint" of the flow can be completed by the use of Vapour-Screen. Vortices in the flow can be visualized by this light-sheet technique. Herein condensed water droplets are used as tracer particles. To begin with wet air is used as fluid. During a test humidity condenses and forms a uniform screen in the flow. This technique was first introduced by McGregor (1961) for visualization in wind tunnels.

Quantitative measurements are then carried out by velocity measurements. Particle-Image-Velocimetry (PIV) is a technique which determines fluid velocities by measuring particle velocities in the flow. It is applied in a set of light sheets to obtain all three velocity components in a volume of the flow by combining the data from the different planes of measurement. PIV is applied to a $Ma_\infty = 2$ supersonic flow the first time. Therefore it is of fundamental importance to examine the flow tracking capabilities of these particles too.

2. TEST FACILITY AND MODELS

Flow visualization and PIV-measurements are carried out in the trisonic wind tunnel of the Aerodynamisches Institut Aachen (AIA). It is a suction type wind tunnel with a test section size of 40x40 cm^2. During a run the air is sucked from the balloon through the Laval nozzle, then the test section and finally through the diffuser into the vacuum tanks, see Figure 3. It is a intermittent working wind tunnel, which enables testing times of about 3 s at $Ma_\infty = 2$.

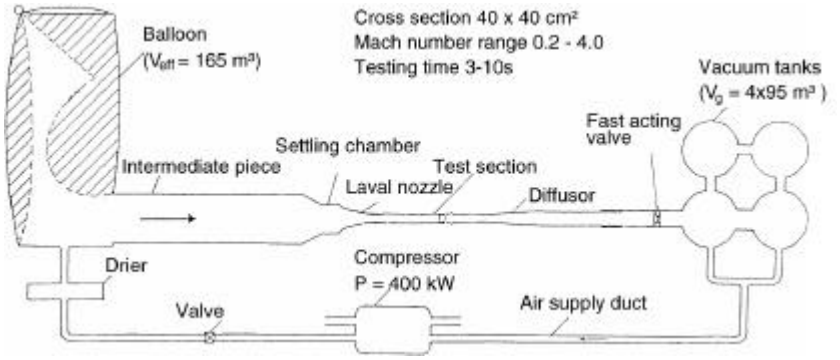

Figure 3: Trisonic wind tunnel of the Aerodynamisches Institut Aachen (AIA). This intermittent suction type wind tunnel enables Mach numbers from Ma = 0.2 to 4 and testing times of about 3 s.

Two different models of the first stage ELAC are used for the tests. Flow visualization at a relative chord length of x/l = 30% is carried out with the help of a 1:100 scaled model. It is a submodel of the first 40% of this configuration. This allows an accurate reconstruction of the leading edge geometry of ELAC, which is an important aspect at flow separation. The corresponding Reynolds number is $Re_\infty = 8.9\times10^6$ at $Ma_\infty = 2$. Reynolds number and Mach number are interdependent in a suction type wind tunnel. Therefore the Reynolds number was $Re_\infty = 7.0\times10^6$ at $Ma_\infty = 2.5$.

The qualitative investigation of the flow around the control surfaces of ELAC and the PIV measurements are carried out with a 1:240 scaled model. It is shown in Figure 4: A delta-shaped lifting body with a sweep-back angle of 75°. It has rounded leading edges to reduce the heat flux at hypersonic flight conditions. The control surfaces are located at the rear of the wing, starting at x/l = 80%. The Reynolds number are $Re_\infty = 3.7\times10^6$ at $Ma_\infty = 2.0$ and $Re_\infty = 2.9\times10^6$ at $Ma_\infty = 2.5$.

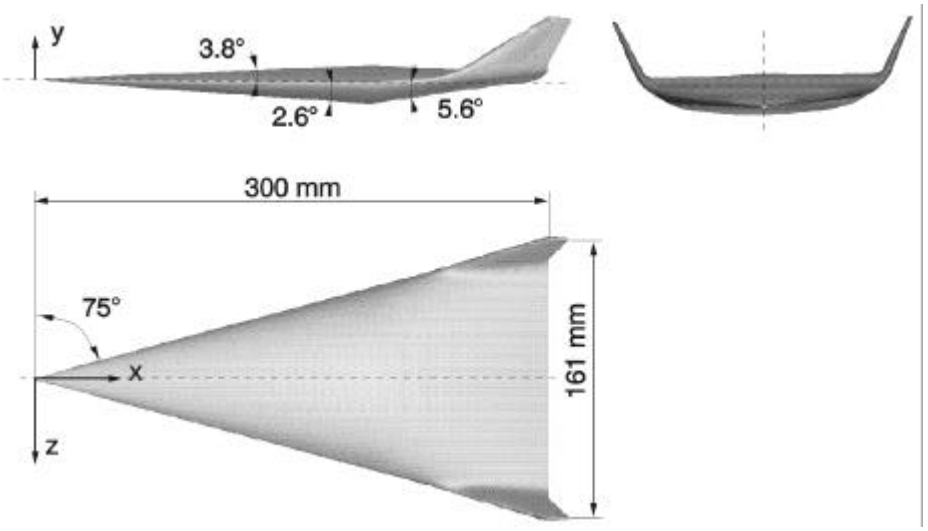

Figure 4: Model of the first stage ELAC scaled 1:240 designed for the wind tunnel test in the trisonic wind tunnel of the Aerodynamisches Institut Aachen.

3 FLOW VISUALIZATION USING VAPOUR-SCREEN

Generally light sheet techniques for flow visualization of vortices in the flow field are realized with indicators, which are added to the fluid. Usually smoke is used as such an indicator for tests in low-speed wind tunnels. The initial uniform distribution of the indicator in the flow field is disturbed by forces acting on the smoke particles. Vortices with its centrifugal forces move the indicator particles away from the vortex centre. This non-uniform distribution can be visualized by illuminating a plane of the flow field. This plane is recorded with a camera. Vortices appear as dark areas on the image, because the amount of scattered light in a vortex is less due to a lower particle concentration. The whole flow field can be visualized by this method, if planes at different positions are recorded.

In supersonic flow fields problems concerning the particle generation are caused by high velocities in the flow. A large number of particles is necessary for a concentration which ensures a sufficient contrast on the recorded images. Applying the Vapour-Screen technique solves this problem. Scattering particles are produced by condensation of wet air. In supersonic flow the fluids humidity condenses downstream of the minimum cross section. The condensation is caused by dropping pressure and temperature, its onset is situated next to the minimum cross section of the wind tunnels Laval nozzle. The process forms a uniform droplet distribution between the Laval nozzle and the test section. This technique was first applied by Allen and Perkins (1951). Later McGregor (1961) used this method to visualize the leeside vortices of a wing at $Ma_\infty = 1.75$ at different angles off attack, see Figure 5.

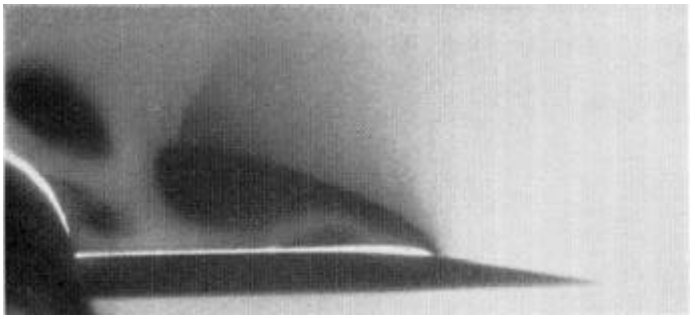

Figure 5: Flow visualization of leeside vortices over a wing using the Vapour-Screen technique at $Ma_\infty = 1.75$ at 18° angle of attack from McGregor (1961).

The phase transformation of humidity has an influence on the flow field. The latent heat resulting from the condensation process is added to the fluid. Therefore it is advisable to ensure a completed condensation in front of the test section. Furthermore the laws of one-dimensional gas dynamics must be extended to describe this flow with heat transfer and its influence on stagnation Temperature T_0. Still the flow field is isentropic up to the onset of condensation. It is a homogeneous non-equilibrium process, if $Ma_\infty < 1.5$. In this case condensation nuclei are caused by strong oversaturation. The area of condensation is situated downstream of the minimum cross section dependent on the relative humidity of the fluid φ_0 at stagnation condition. The investigation of Schnerr and Zierep (1996) shows, that steady flow is achieved when $\varphi_0 \leq 40\%$. Figure 6 shows results from numerical simulation of the condensation process in a Laval nozzle. Condensation nuclei are formed next to the minimum cross section over a distance of approx. 20 mm. Then the size of these initial droplets increases because of the continued condensation. This is indicated by the condensate mass fraction in Figure 6. After a total distance of approx. 40-50 mm the condensation process is completed. The initial fluids humidity is now completely condensed and forms a uniform fog in the diverging part of the Laval nozzle.

The condensation process affects the pressure distribution, which is also depicted in Figure 6. Therefore the Mach number in the experiment must be corrected to take the mass transfer and the corresponding heat exchange into consideration. With the help of equations (1) and (2), which were derived by McGregor (1961), a correction of static pressure p and Mach number Ma dependent on condensation Mach number Ma_k and the Mach number without any heat transfer Ma_{dry} is possible. The exchanged heat is q. It is approximately equivalent to the latent heat $x\, r_0$ with the absolute humidity x and the heat of vaporization r_0. Figure 7 shows a correction for the Mach number dependant on equations (1) and (2) for the mentioned stagnation state. The shape of the adjustable Laval nozzle must be corrected corresponding to Figure 7b.

$$\frac{p}{p_{dry}} = 1 + \frac{1}{2}\left[\frac{k\, Ma_{dry}^2}{Ma_{dry}^2 - 1}\left(1 + k\, Ma_k^2\right) - k\, Ma_k^2\right]\frac{q}{c_p T_0} \qquad (1)$$

$$\frac{Ma}{Ma_{dry}} = 1 - \frac{1}{2}\left[\frac{(1 + k\,Ma_k^2)\left(1 + \frac{1}{2}(k-1)Ma_{dry}^2\right)}{Ma_{dry}^2 - 1}\right]\frac{q}{c_p T_0} \qquad (2)$$

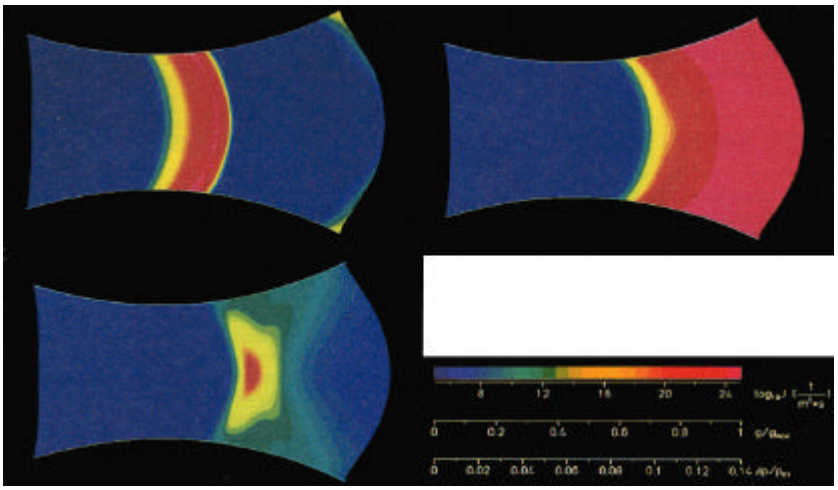

Figure 6: Simulation of the homogeneous condensation process in a Laval nozzle in supersonic flow from Schnerr and Zierep (1996). Homogeneous nucleation rate, condensate mass fraction (upper part), static pressure disturbance and colour chart for the numerical results.

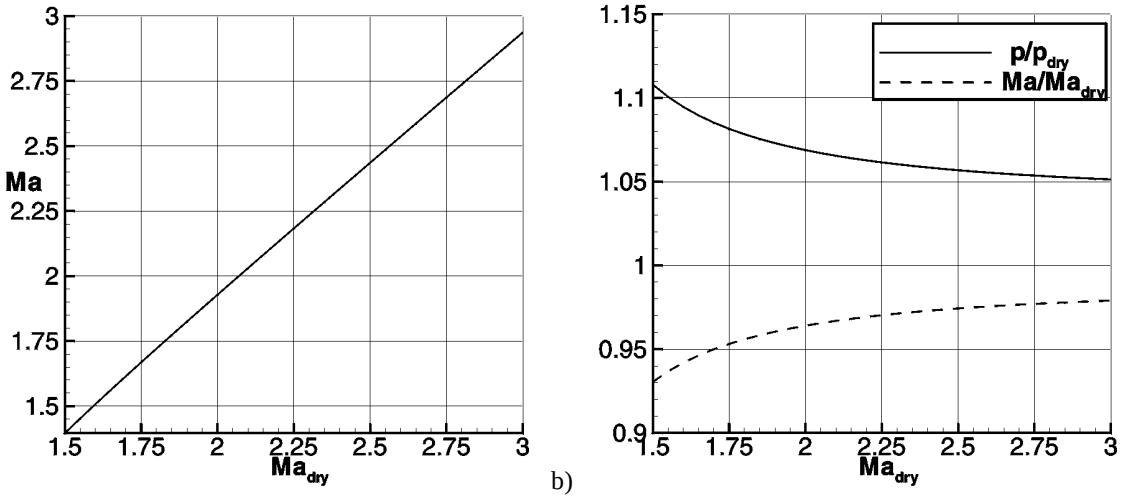

Figure 7: a) Correction of the Mach number Mach number Ma dependent on the Mach number without condensation Ma_{dry} and b) influence of the condensation process on the static pressure p with $p_0 = 10^5$ Pa, $T_0 = 298$ K and $j_0 = 25\%$.

3.1 Experimental set-up

A laser-light sheet is used to visualize the droplet concentration in the flow field. It is realized by the use of a 5W cw-argon-ion laser and an appropriate light sheet optic with a focussing telescopic lens system and a cylindrical lens to expand the laser beam to a plane. The so generated light sheet is orientated perpendicular to the model surface to visualize the vortices over the leeside of the delta wing. The illuminated plane is recorded with the help of a greyscale CCD camera. Its resolution is 512×582 Pixels with 8 bit depth of shade. The recorded image is distorted, because image plane and light sheet are tilted, see Figure 8. This problem is solvable by recording a calibration grid, so that the images can be rearranged to give a correct impression of the flow field.

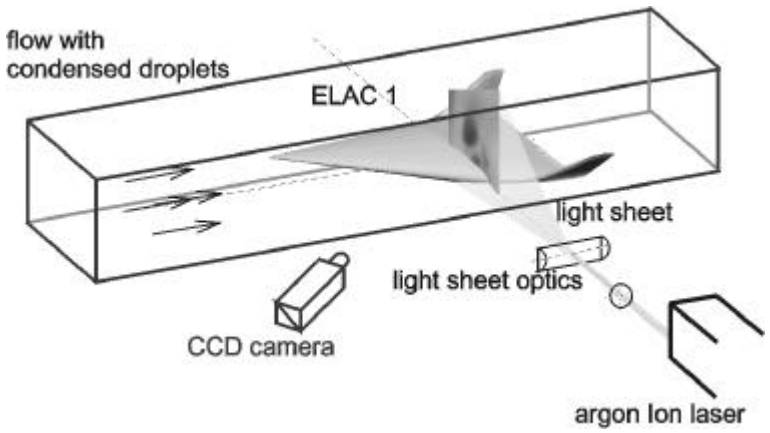

Figure 8: Experimental set-up for the Vapour-Screen technique using a light sheet optic and a cw-laser. The illuminated plane is recorded with a CCD camera.

An improved visualization of the images can be achieved by manipulating the colour map of the image in the area of the different vortices. If the image contrast in these areas is small, the different grey levels can be alternately replaced by black and white. Especially small vortices in the flow field can be visualized clearly by this method. An example of the changed colour map of a Vapour-Screen image is shown in Figure 9.

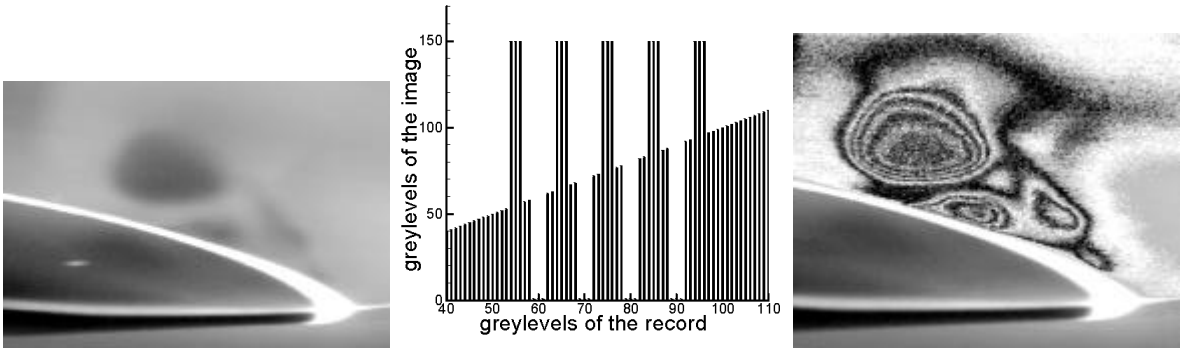

Figure 9: Image processing for the enhanced visualization of vortices in a Vapour-Screen image. Left: Original of a Vapour-Screen image. The dark areas representing the vortex structure are emphasized by changing the colourmap (centre). The improved image shows clearly the vortex system over the leeside of the wing (right).

4 VELOCITY MEASUREMENTS USING PARTICLE-IMAGE-VELOCIMETRY

Particle-Image-Velocimetry is a technique to measure the velocity distribution in a fluid. Small particles are added to the fluid and their velocity is measured by recording their position at different times. Usually a pulsed laser system is used to illuminate a plane of the flow field. Then this plane is recorded with the help of a camera.

4.1 Experimental set-up

When PIV is applied to a supersonic field the time interval Δt between the laser light pulses must be very small. When a medium with high resolution as e.g. a photographic film is applied to enable measurements with high spatial resolution, images cannot be recorded separately for very small Δt. Thus the particles in the flow field are recorded twice on one image. These images are evaluated using a semi-optical system. The image is subdivided in small sections which are known as interrogation spots. The spots are sequentially illuminated with a cw-laser to generate Youngs fringes. These form an interference figure containing information about the most frequent distance between the particles pairs recorded at t and $t+\Delta t$ in the interrogation spot. A second inverse Fourier transform results in the autocorrelation plane and finally the velocity vector, which corresponds to the location of the interrogation spot. The sequence of this evaluation process is illustrated in Figure 10.

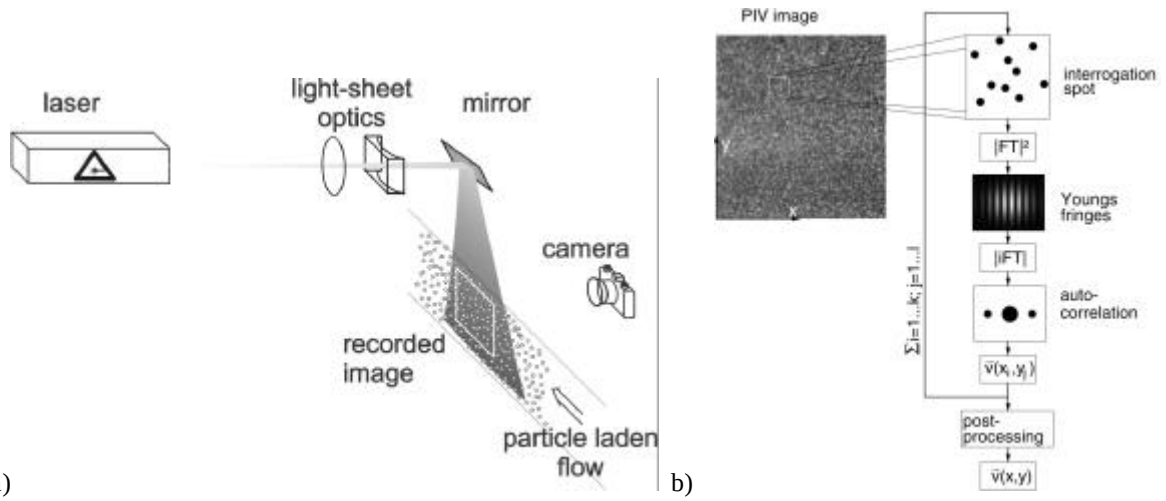

a) b)

Figure 10: Left: Principle of velocity measurement using Particle-Image-Velocimetry. The motion of particles in a fluid flow is recorded and thus the surrounding fluid velocity measured. Right: Evaluation of PIV images with a semi-optical system using autocorrelation.

The experimental set-up for the velocity measurements using PIV in the trisonic wind tunnel of the Aerodynamisches Institut Aachen is shown in Figure 11. The short pulses distances Δt of the light sheet are realized by the use of double-cavity Nd:YAG laser with 170 mJ per pulse at 532 nm. Two telescopic optics and a cylindrical lens form the light sheet, which is cast from the top through the housing of the wind tunnel and the Laval nozzle into the test section. Olive oil droplets are used as tracer particles. These are generated with the help of two aerosol generators, each containing 18 Laskin nozzles. The particles mean diameter is 1.95 µm. Images of the pulsed light sheet are taken as a side view from the test section with a 60 mm lens and a high-resolution technical pan film. Combining measurements at different positions of the light sheet over the leeside of the model all three velocity components can be obtained in a volume of the flow field. Thus the spatial development of the vortex system can be examined.

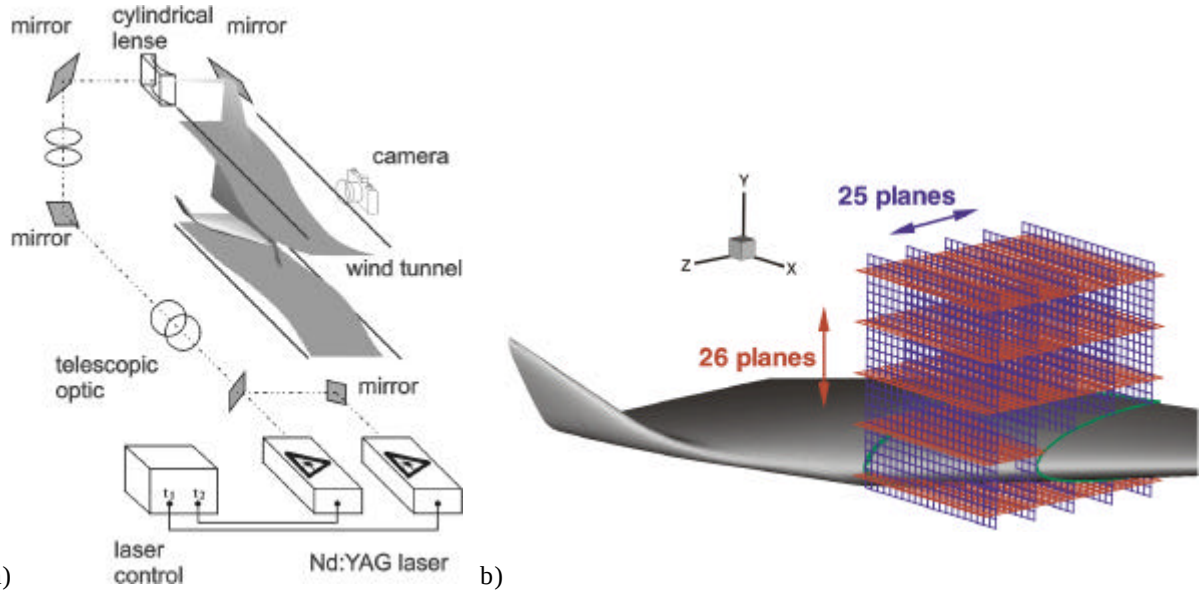

a) b)

Figure 11: a) Experimental set-up for the application of PIV to the trisonic wind tunnel of the Aerodynamisches Institut Aachen. The light sheet is generated with the help of a double-cavity Nd:YAG laser, two telescopic optics and a cylindrical lens. b) Orientation of the different planes of measurement over the leeside of the ELAC configuration.

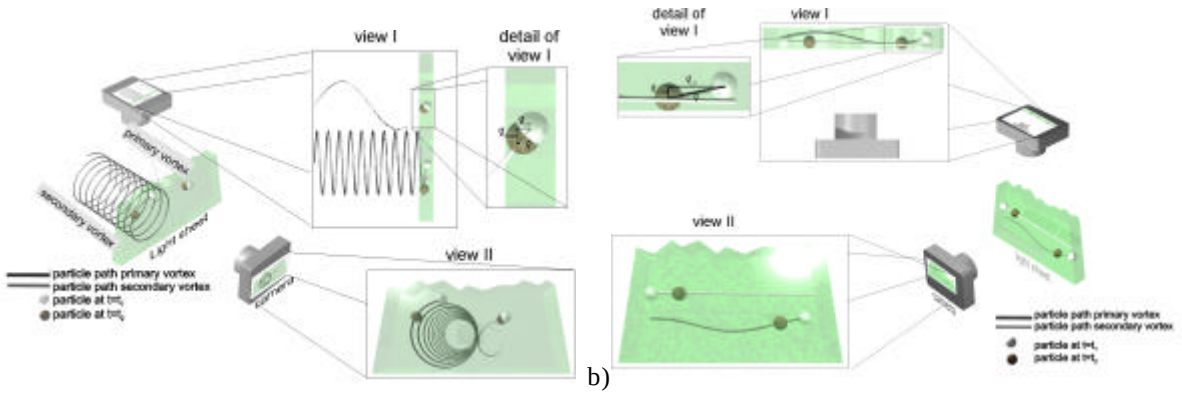

a) b)

Figure 12: Different arrangements to measure the velocity distribution with PIV in a flow field containing vortices with different circumferential velocities, which are caused e.g. by primary and secondary separation of the flow. a) Light sheet perpendicular to the vortex axis: This set-up makes velocity measurements in the area of the secondary vortex impossible, because the different particle images overlap on the record (view II). b) A side view recording technique allows the measurement of all three velocity components, especially in the area of the secondary vortex.

When PIV is applied to a vortical flow field the orientation of light sheet and recording system is very important to obtain a correct image of the flow field. Figure 12 describes two different arrangements for PIV measurements. When double exposed images are recorded, a light sheet orientation perpendicular to the vortex axis results in overlapping particle images in the area of the secondary vortex, where the circumferential velocity is less than in the primary vortex. It is possible to cope with this problem by orientating the light sheet in main flow direction. Combining both side and top view, all velocity components will be correctly measured and information also in the area of the secondary vortex is gained.

4.2 Flow tracking capabilities

The ability of tracer particles to follow the fluid are of fundamental importance, when PIV is applied to a supersonic flow field. Large velocity gradients in the flow field as e.g. shock waves call for high demands on the tracking capabilities. The particle paths in a given flow field can be computed by applying the Basset-Boussinesq-Oseens equation (BBO). According to Newton's second law the left hand side of equation (3) is the product of particle mass and acceleration. It equals to the external forces on the right hand side being drag, gravity, pressure gradient force, virtual mass and Basset force, see Maxey and Riley (1983).

$$\frac{1}{6}\pi\rho_p d_p^3 \frac{du_p}{dt} = \frac{1}{8}\pi\rho_f d_p^2 \mathrm{Re}_p c_D (u_f - u_p) + \frac{1}{6}\pi d_p^3 (\rho_p - \rho_f) g + \frac{1}{6}\pi d_p^3 \rho_f \frac{\partial p}{\partial x_i}$$
$$+ \frac{1}{12}\pi d_p^3 \rho_f \frac{d}{dt}\left(u_f - u_p\right) - \frac{3}{2}\pi d_p^2 \sqrt{\pi\rho_f \mu} \int_{t_0}^{t} \frac{d/dt\left(u_f - u_p\right)}{\sqrt{t - t_0}} dt + \sum F_i \qquad (3)$$

The subscripts *f* and *p* represent particle and fluid relevant variables. Velocity and density are denoted by *u* and ρ, the viscosity of the fluid by η. Re_p is the particle Reynolds number. An estimate of the order of magnitude of the different terms shows, that most of the external forces can be neglected, when particle motion in a supersonic flow field is to be investigated, see Lang (1998,2000). Thus particle motion downstream of an oblique shock is sufficiently described by equation (4).

$$\frac{\partial u_p}{\partial t} = -\frac{3}{4}\mathrm{Re}_p c_D \frac{\rho_f}{\rho_p d_p^2}\left(u_p - u_f\right) \qquad (4)$$

Solutions of this equation are presented in Figure 13. The computed motion of particles downstream of an oblique shock for different c_D-formulations is compared with PIV measurements. The oblique shock in the experiment is generated by a flat plate with sharp leading edge at $Ma_\infty = 1.98$ and an angle of attack of $\alpha = 6.25°$. Both experiment and computation show a velocity lag of the particles of approximately 8-10 mm downstream of the shock until they come up with the fluid velocity.

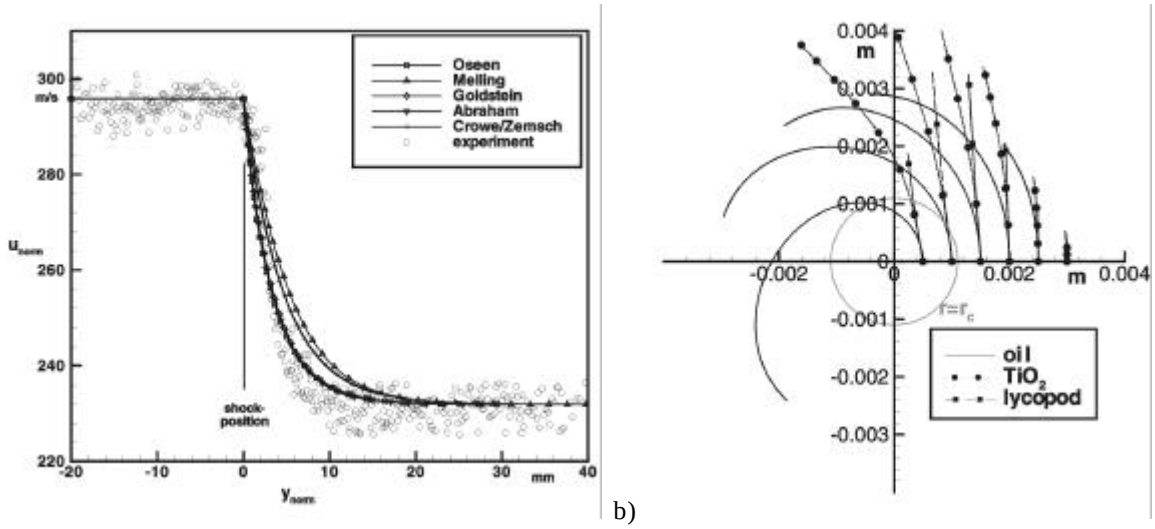

a) b)

Figure 13: a) Motion of particles downstream of an oblique shock generated by a flat plate at $Ma_\infty = 1.98$ and $\alpha = 6.25°$. The different lines indicate the computed particle motion. The symbols show results from PIV measurements. At approximately 8-10 mm downstream of the shock, particles get the fluid velocity. b) Paths of different types of particles in a compressible wing tip vortex, which was estimated by Oseen's vortex model. Increasing density (TiO_2) and size (lycopod) have a negative effect on the flow tracking capabilities of the particles.

The particle motion in a vortex can be described by equations (5) and (6). It is a simplified BBO-equation in cylindrical coordinates. A numerical solution of these equations is obtained by the application of a 5th order Runge-Kutta method.

$$\frac{\partial u_{p,r}}{\partial t} = \frac{u_{p,\Theta}^2}{r} - \frac{1}{r_p}\frac{\partial p}{\partial r} - \frac{3h}{4 r_p d_p^2} c_D \,\mathrm{Re}_p \, u_{p,r} \qquad (5)$$

$$\frac{\partial u_{p,\Theta}}{\partial t} = -\frac{u_{p,r} u_{p,\Theta}}{r} + \frac{3h}{4 r_p d_p^2} c_D \,\mathrm{Re}_p \left(u_{f,\Theta} - u_{p,\Theta}\right) \qquad (6)$$

The computed particle paths are shown in Figure 13b for a wing tip vortex in compressible flow according to the experiments of Bershader (1987). Different types of particles are used in the computation. Particle of higher density and larger diameter show a decline in comparison to the used olive oil droplets. Due to centrifugal forces, the particles move towards bigger diameters. The effect on the quality of PIV measurements is described more detailed in Lang (2000).

5. RESULTS

5.1 Flow visualization

A combination of oil flow pattern and Vapour-Screen show the spatial development of the vortex system over the leeside of the delta wing. The oil flow pattern indicates the areas of separation and reattachment of the flow. Furthermore the sense of rotation is illustrated by the remaining structure on the body's surface. But weak vortices may not occur in this flow pattern.

Figure 14 shows Vapour-Screen images at $x/l = 30\%$ at $Ma_\infty = 2$ and 2.5. A free shear layer containing the primary vortex can clearly be seen. Flow separates next to the leading edge and rolls-up into this dominating vortex. When Ma_∞ is increased to 2.5, Re_∞ decreases to 7.0×10^6. Then primary separation and reattachment move towards the centre line of the model. The reattachment is shifted in the same direction by a broader and flat primary vortex. A secondary vortex is not indicated by the Vapour-Screen, but the oil flow pattern shows its fingerprint on the model's surface. When α is increased, the secondary vortex is to be seen in the Vapour-Screen image, see e.g. the visualization at $Ma_\infty = 2$ and $\alpha = 15°$ in Figure 9.

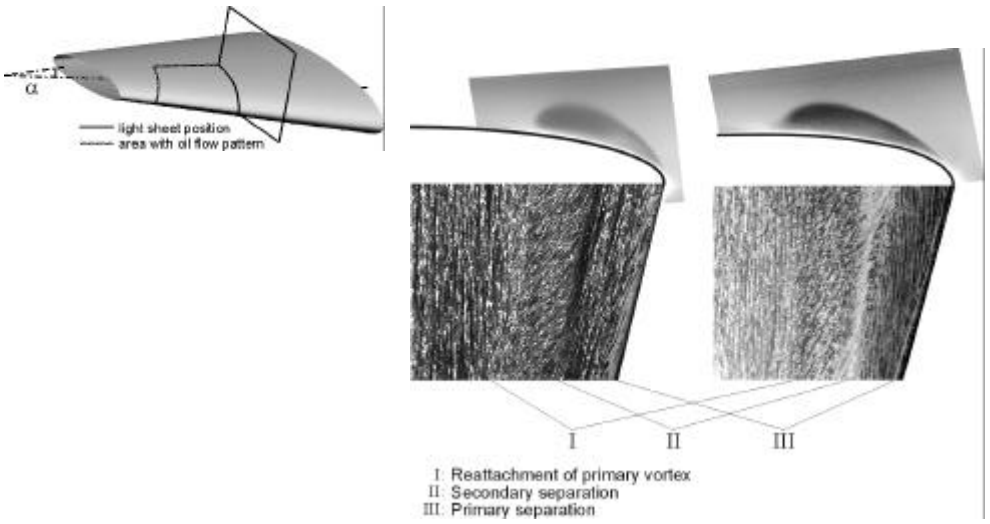

Figure 14: Vapour-Screen image (upper part) and oil flow pattern (lower part) at the hypersonic configuration ELAC at a = 9°, Ma_∞ = 2 (left) and a = 9°, Ma_∞ = 2.5 (right). Primary separation is to be seen near to the leading edge and the corresponding reattachment of the flow at I. The secondary separation is also indicated by the flow pattern. A broad and flat primary vortex is generated when the Mach number is increased.

The spatial development of the vortex system between the control surfaces is shown in Figure 15 for different Mach numbers. The primary vortex gets an egg-shape up to the end of the wing. This is caused by the changed geometry of the leading edges of the control surfaces. In the corner of delta wing and control surface flow separates due to the shock, which is generated by the change of the leading edge. The shock is indicated by the Vapour-Screen images. The separated area contains a clockwise rotating vortex, which is depicted by the oil flow pattern.

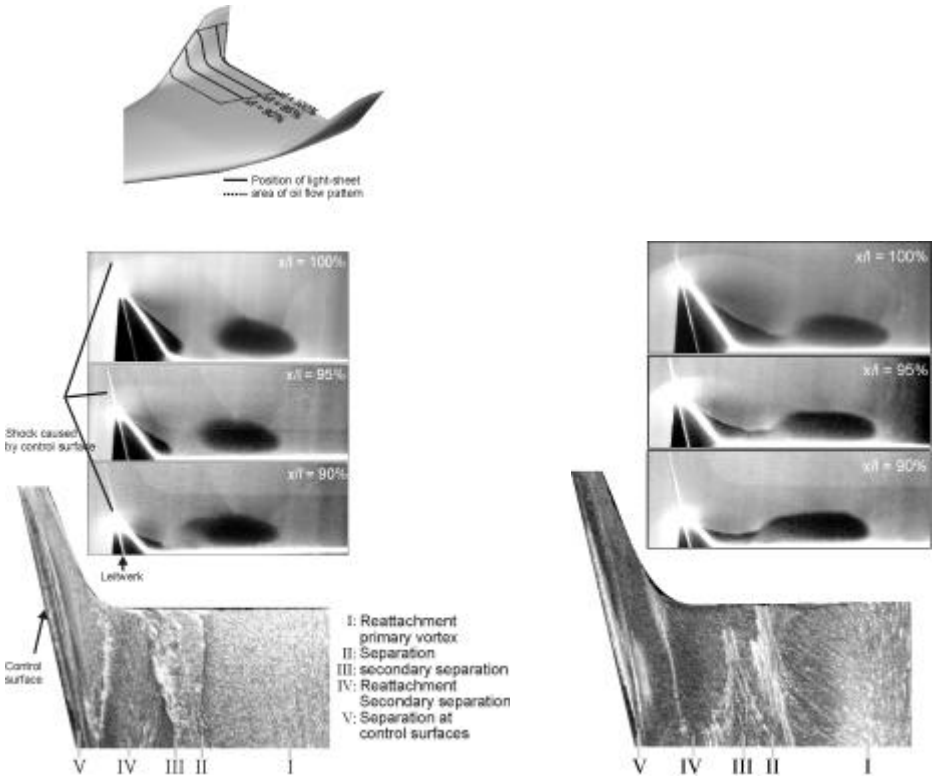

Figure 15: Vapour-Screen image (upper part) and oil flow pattern (lower part) between the control surfaces of ELAC at a = 10°, Ma_∞ = 2 (left) and a = 10°, Ma_∞ = 2.5 (right). Due to the changing geometry of the leading edge the shape of primary vortex changes. Inside of the control surface an area with separated flow is indicated.

According to these results a vortex topology can be developed, which fulfils the topological rules of Peake and Tobak (1980). They determine the number of saddle points, foci, half-saddles and half-nodes which are necessary to postulate a correct vortex system. The topological sketches show a plane of the three-dimensional flow field and illustrate clearly the structure of the flow. Figure 16 shows the so developed vortex topology of the ELAC configuration. At moderate α (α[15°) two vortices (F_1 anf F_2) occur in the front and a further vortex at the rear of the wing.

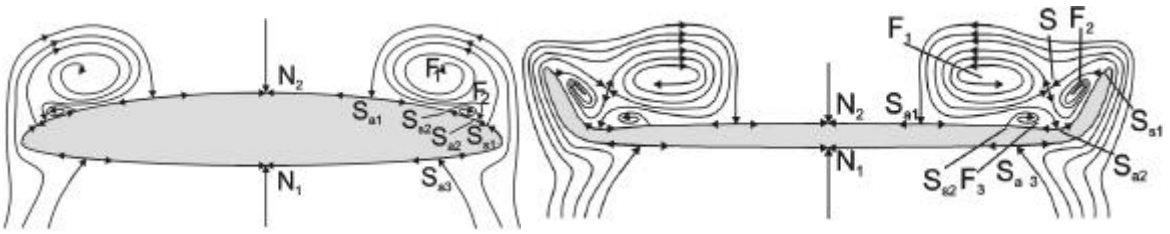

Figure 16: Vortex topology for the ELAC configuration according to the topological rules of Peake and Tobak (1980) for the front part of the wing (left) and the rear part between the control surfaces (right). Separation is indicated by S_{si}, attachment by S_{ai}, vortices (foci) by F_i, saddle points by S and half-nodes by N_i.

If the colour map of Vapour-Screen images is changed according to Figure 9, measurements can be used for data validation of results from numerical simulation. These are shown in form of isolines of vorticity. A good agreement concerning size, shape and position of vortices can be achieved.

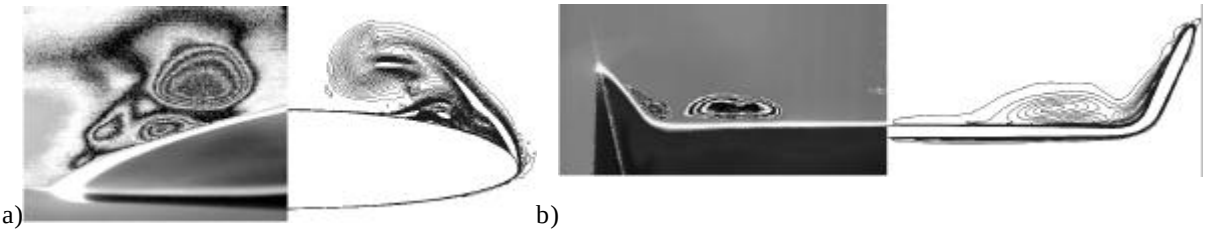

Figure 17: Comparison of Vapour-Screen images with changed colour map as described in Figure 9 and iso-vorticity lines of numerical computations from Henze (1996) at x/l = 66%, a = 15° (a) and x/l = 95%, a = 10° (b).

5.1 Velocity measurements

PIV measurements provide all three velocity components over the leeside of the delta wing, because measurements from a set of light sheets were combined. The cross flow planes show the roll-up of the free shear layer into the primary vortex, see Figure 18. The corresponding vorticity distribution shows the convective transport of vorticity from the boundary layer into the vortex core.

The spatial development is also to be seen in the upper part of Figure 19: It shows the vorticity distribution in several cross flow planes and an isosurface of vorticity. Due to viscous effects the cross section size of this tube decreases, while it is fed by flow separation at the leading edge. This can only be observed in the vortex core. But the vortex strength itself increases in main flow direction as proved by plotting the circumferential velocity versus the distance from the vortex centre at different chord lengths. Increasing size and velocity verify an increasing vortex strength, because the corresponding circulation Γ increases. Also an almost conical characteristic is detected: The ratio of vortex core diameter and span remains approximately constant.

Figure 19 shows a comparison of measurements and numerical simulation too. Again numerical results are confirmed. They show the same behaviour of the vorticity distribution in the vortex core in main chord direction, as observed in the experiment. Due to the higher resolution of the numerical data, the transport of vorticity is there to be seen very clearly.

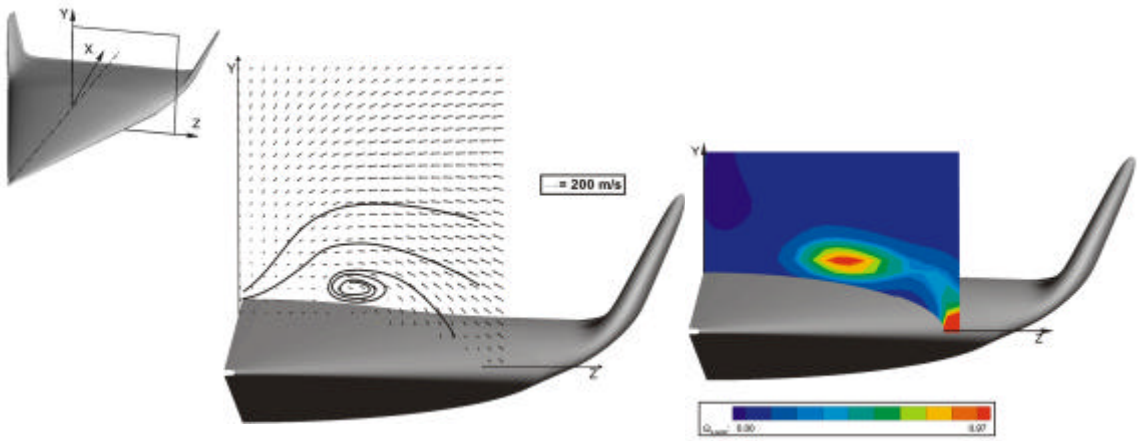

Figure 18: Distribution of the non-conical velocity components and vorticity in a cross flow plane over the leeside of ELAC at $Ma_\infty = 2$ and $\alpha = 10°$. The streamlines in the cross section illustrate the roll-up of the shear layer into the primary vortex. The dimensionless vorticity W depicts the convective transport of vorticity into the primary vortex.

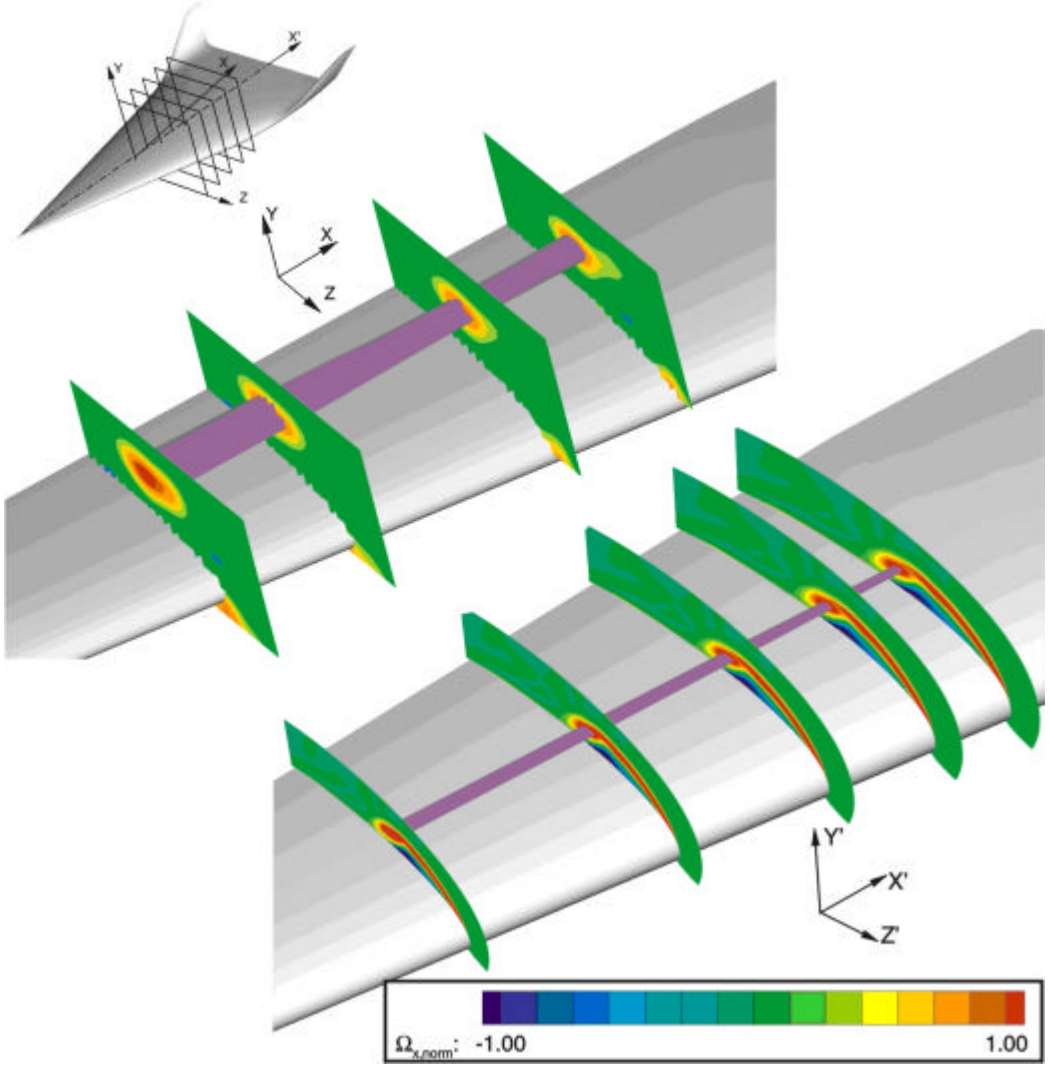

Figure 19: Spatial development of the primary vortex in main flow direction. Vorticity distribution is shown in several cross flow planes and the extracted isosurface of vorticity shows decreasing vorticity, which is caused by viscous effects in the vortex core. Top: Vorticity distribution computed with the results from PIV measurements and vorticity distribution of the numerical simulation from Henze (1996) (bottom).

REFERENCES

Allen, H.J. and Perkins, E.W. (1951). “A study of effects of viscosity on flow over slender inclined bodies of revolution”, NACA Technical Report No. 1048.

Bershader, D. (1987). “Shock Tube Studies of Vortex Structure and Behaviour”, in Grönig, H., “Shock Tubes and Waves”, VCH Verlagsgesellschaft, Weinheim, Germany, pp. 5-18.

Henze, A., Houtmann, E.M., Jacobs, M. and Vetlutsky, V.N. (1996). “Comparison between experimental and numerical heat flux data for supersonic flow around ELAC 1”, Zeitschrift für Flugwissenschaft und Weltraumforschung., Vol. 20, pp. 61-70.

Lang, N. (2000). “Sichtbarmachung und Geschwindigkeitsmessung in Leeseitenwirbeln bei Überschallan-strömung“, Ph.D. thesis, Aerodynamisches Institut, RWTH Aachen, Germany.

Lang, N. (1999). “Investigation of the flow tracking capabilities of tracer particles for the application of PIV to supersonic flow fields“, in Körner, H. and Hilbig, R. “New Results in Numerical and Experimental Fluid Mechanics“, Notes on Numerical Fluid Mechanics Vol. 72, pp. 266-273. Vieweg.

Maxey, M.R. and Riley, J.J. (1983). “Equation of motion for a small rigid sphere in a nonuniform flow”, Physics of Fluids, Vol. 26, No. 4, pp. 883 – 889.

McGregor, J.(1961).“The Vapour-Screen method of flow visualisation”, Journal of Fluid Mechanics, Vol. 11, No. 4, pp. 481-511.

Miller, D.S. and Wood, R.M. (1984) “Leeside flows over delta wings at supersonic speeds”, Journal of Aircraft, Vol. 21, pp. 680—686

Peake, D.J. and Tobak, M. (1980). “Three-dimensional interactions and vortical flows with emphasis on high speeds”, AGARD-AG-252.

Schnerr, G.H. and Zierep, J. (1996). “Condensation phenomena in Laval nozzles”, In: Nakayama, Y. and Tanida, Y., “Atlas of Visualization”, pp. 151-165. CRC Press, Boca Raton.